Estimates of earthquake temperature rise, frictional energy, and implications to earthquake energy budgets

Supplementary material

S1. Thermal modelling

To constrain the temperature rise associated with a given MPI4 and CPI, heat generation and diffusion equations (Carslaw & Jaeger, 1959; Lachenbruch, 1986) for a fault are coupled with the reaction kinetics for MPI4 and CPI (Rabinowitz et al., 2017; Sheppard et al., 2015). The adiabatic temperature rise that occurs depends on properties of the fault zone, inside the fault zone it is as follows:

$$\Delta T(x<a,t)=\frac{\tau}{\rho c}\frac{v}{2a}\left\{t\left[1-2i^2erfc\frac{a-x}{\sqrt{4\alpha t}}-2i^2erfc\frac{a+x}{\sqrt{4\alpha t}}\right]-H(t-t^*)(t-t^*)\left[1-2i^2erfc\frac{a-x}{\sqrt{4\alpha(t-t^*)}}-2i^2erfc\frac{a+x}{\sqrt{4\alpha(t-t^*)}}\right]\right\} \quad (1)$$

where x is distance from the midpoint of the fault, t is time, t^* is the duration of the event, τ is shear stress, v is slip velocity, a is the half-width of the slip layer, ρ is density, c is heat capacity, δ is thermal diffusivity, and i^2erfc is the second integral of the complementary error function. $H(\varsigma)$ is the Heaviside function evaluated for $\varsigma = t - t^*$. Parameters used in this calculation can be found in Supplementary table 1. Thermal diffusivity of material on either side of the slip surface is assumed to be the same. Outside of the actively slipping layer, temperature rise is described as:

$$\Delta T(x>a,t)=\frac{\tau}{\rho c}\frac{v}{2a}\left\{t\left[2i^2erfc\frac{x-a}{\sqrt{4\alpha t}}-2i^2erfc\frac{x+a}{\sqrt{4\alpha t}}\right]-H(t-t^*)(t-t^*)\left[2i^2erfc\frac{x-a}{\sqrt{4\alpha(t-t^*)}}-2i^2erfc\frac{x+a}{\sqrt{4\alpha(t-t^*)}}\right]\right\} \quad (2)$$

Supplementary Table 1 – thermal and fault parameters used to model heating in the new faults measured here

Fault	c_p (J/K.kg)	α (s^{-1})	ρ (kg/m^3)	z (m)	2a (mm)	Reference
Spoleto	962	1.3E-06	2710	2500	0.3 - 1	Collettini et al. (2013), Waples & Waples, (2004)
Marin	860	0.9E-06	2700	6000	1 - 4	Robertson (1988), Di Toro et al. (2011), Regalla et al. (2018), Waples & Waples (2004)
Nankai	910	1.00E-06	2000	271, 438	10, 2	Saffer et al. (2017), Di Toro et al. (2011), Waples & Waples (2004), Sakaguchi et al. (2011)
Hundalee	775	1.3E-06	2600	1000 - 10000	10 - 20	Williams et al. (2018), Waples (2004)
Nojima (Mugi, Okitsu)	1090	0.8E-05	2600	3200-4000, 4000-6000	0.6-1.5	Ujiie et al. (2007), Waples & Waples, (2004), Robertson (1988)
Skeeter	1040	1.5E-6	2800	4200	0.25-1	Kirkpatrick et al. (2012), Heuze (1983), Waples & Waples, (2004)
Wasatch Damage Zone	980	0.9E-6	2800	1500	0.1-2	Mcdermott et al. (2017). Heuze (1983), Waples & Waples, (2004)

In most of these faults shear stress and displacement are unknown, we use a range of reasonable shear stress values calculated using estimates of depth and a uniform distribution of friction between peak and steady state friction estimated from the literature. A uniform distribution of displacements is also used to model the possible events on the fault. In the case of the Hundalee fault, we have estimates of displacement from the Kaikoura sequence and by using a coefficient of variation of 0.5 (Hecker et al., 2013) we use this to guide thermal modelling. However, we do not know the depth that these faults are active so we use a uniform distribution of depths along with friction to model the possible heating scenarios here. Temperature profiles are then coupled with biomarker reaction kinetics (Sheppard et al., 2015; Rabinowitz et al., 2017) using the Easy%R method (Sweeney & Burnham, 1990) modified for a single reactant. The original Easy%R method uses multiple parallel reactions to model the complex reactions leading to vitrinite maturation. Our modification uses the same underlying integration of reaction extent. However, we use a single reaction to describe a particular biomarker parameter and model the extent of reaction from a time-temperature input. A Monte Carlo approach is used to propagate uncertainties in the reaction kinetics and the uncertainties in fault thickness, displacement, and shear stress. We can then identify the MPI4 and CPI profiles that best fit sample measurements and the extraction of possible coseismic temperatures.

S2. Biomarker thermal maturities background:

Methylphenanthrene Index (MPI-4)

Methylphenanthrenes are polycyclic aromatic hydrocarbons produced by diagenesis of pre-existing organic material (Peters et al., 2007). Changes in methylphenanthrene isomer abundance occurs with increasing temperature (Szczerba & Rospondek, 2010). 2- and 3-methylphenanthrene (2MP, 3MP) are thermally stable methylphenanthrene isomers and increase in abundance during heating. 9- and 1-methylphenanthrene (9MP, 1MP) on the other hand, are the thermally unstable isomers. Using the abundance of these we can quantify thermal maturity through MPI-4, as follows:

$$MPI - 4 = \frac{3MP + 2MP}{3MP + 2MP + 9MP + 1MP} \quad (3)$$

Carbon Preference Index (CPI)

n-Alkanes are linear hydrocarbons derived from a variety of sources and they, too, change in abundance with increasing temperature (Peters et al., 2007). Biosynthetic production of long-chained n-alkanes have a preference towards odd-over-even carbon chain lengths which is quantified by the carbon preference index (CPI):

$$CPI = \frac{C25+C27+C29+C31+C33}{C26+C28+C30+C32+C34} \quad (4)$$

When heated, cracking reactions and the production of *n*-alkanes without this carbon preference occur, leading to a reduction in CPI.

S3. Sampling and Analytical Methods

New biomarker thermal maturity results presented in this paper were measured on samples from the Hundalee, Spoleto and Monte Maggio faults, as well as a thrust in the Marin Headlands (Regalla et al., 2018), and a normal fault in the hanging wall of the Nankai subduction zone. Samples were collected along transects across the fault with material collected from the slipping layer and the surrounding less deformed wall rock (e.g. Coffey et al. 2019).

The Hundalee Fault was one of the many faults that ruptured during the 2016 M_w 7.8 Kaikōura earthquake, hosting 1 m and 1 - 1.2 m of vertical and horizontal displacement, respectively. Five shear zones containing localised slip layers were identified within the fault zone along Te Moto Moto Stream (Birches 1 locality of Williams et al. 2016) and samples were collected from within and outside of these shear zones. The Spoleto and Monte Maggio faults are reverse and normal faults respectively, located in the Northern Apennines of Italy. They occur within limestone formations and each have a millimeter scale polished slipping layer. Samples were collected at outcrops of each of these faults, within the polished layer and into the wall rock. Evidence of coseismic heating along both of these faults has been identified previously by (Carpenter et al., 2014; Collettini et al., 2013) who identified evidence of decarbonation reaction products using Scanning Electron Micrograph (SEM) analysis. The Marin Headlands terrane is located just north of San francisco and consists of an exhumed accretionary wedge with over ten imbricate sheets of low grade metabasalt, chert, and greywacke. Eight samples across one of these imbricate thrusts were collected for biomarker analysis. Finally, the Nankai Trough is located off the coast of Honshu, Japan, and accommodates subduction of the Philippine Sea plate beneath the Eurasion plate. IODP EXP 365, a part of the Nankai Trough Seismic Zone Experiment (NanTroSEIZE) drilled into the accretionary complex here, sampling the hanging wall of the megasplay. Numerous smaller faults were identified within the core collected and one of these, between 350 - 400 m depth, was sampled for biomarker measurement.

A brief overview of laboratory methods for biomarker analysis is given here and a more detailed description, including instrument procedures and solvents used can be found in Coffey et al. (2019). Material collected from each of the outlined faults was subsampled if any localized features or structures were present. Then samples were crushed with a mortar and pestle and Accelerated Solvent Extraction (ASE) was used to separate out the Total Lipid Extract (TLE) of each sample. A recovery standard was added to each TLE. Standard silica gel column chromatography procedures were applied to separate the TLE into aliphatic, ketone, and polar fractions. Gas chromatography mass spectrometry was used on the aliphatic and ketone fractions to measure the abundance of alkane and methylphenanthrene molecules, from which thermal maturity ratios could be calculated.

S4. Calculating displacement and average friction

When calculating displacement and frictional work using the thermal modelling methods outlined in this paper, we employ an average friction and stress during slip. This average value takes into account that friction will evolve from some static friction to steady-state lower friction over a thermal weakening distance. As a result the average friction during slip is displacement dependent (smaller displacements will have higher average friction), and an average friction value is coupled to each displacement during thermal modelling . Average stress is calculated according to Seyler et al. (2020):

$$\tau = \tau_{ss} + (\tau_p - \tau_{ss})e^{-\frac{\delta}{D_{th}}} \quad (1)$$

where τ_{ss} is the steady state shear stress, τ_p is the peak shear stress, and δ is the slip accumulated after the thermal weakening distance, D_{th}. The total displacement is divided up into 1000 bins and the friction and stress in each bin is calculated to compute the average. As the displacement and δ increases, the average friction will decrease as more time is spent sliding at lower friction. The thermal weakening distance, D_{th}, is calculated using values reported in Seyler et al. (2020). Where friction is known and reported in past studies, it is used to calculate the peak and steady-state shear stress. Where it is not known a uniform distribution of static friction between 0.55 - 0.65 and dynamic friction of 0.1 - 0.3 is used.

<u>Supplementary Figures</u>

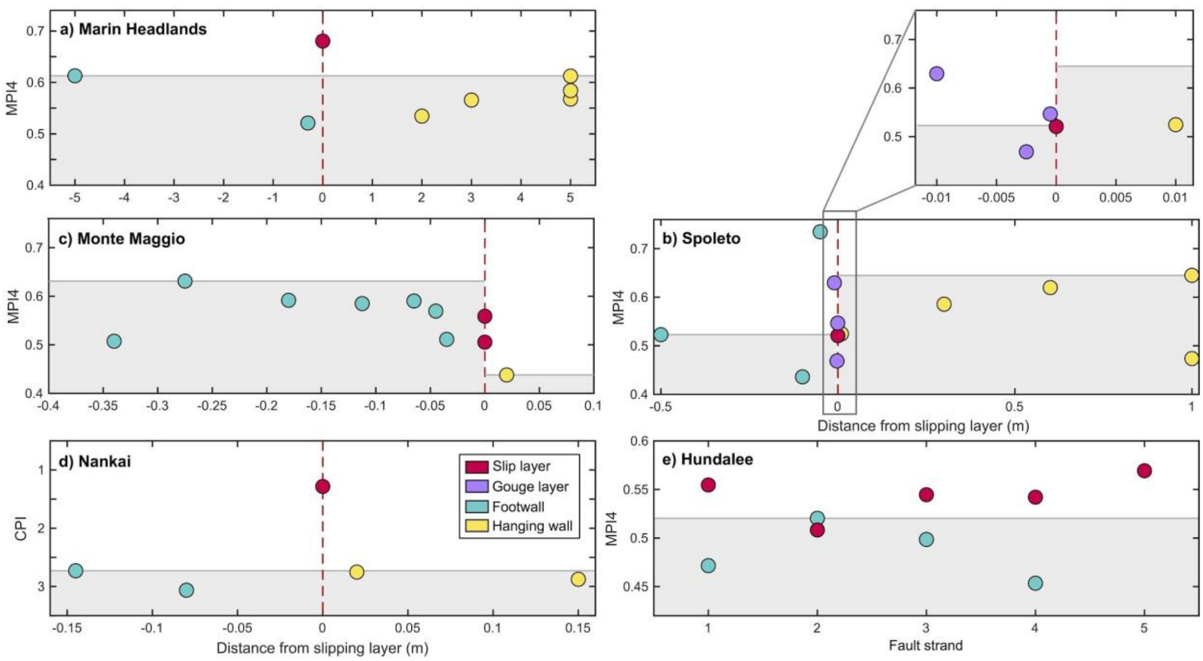

Supplementary Figure 1: Biomarker thermal maturity results for the a) Marin Headlands fault, b) the Spoleto thrust, c) the Monte Maggio fault, d) a thrust fault in the hanging wall of the Nankai subduction zone, and e) strands of the Hundalee Fault. No clear thermal maturity *signal was observed in the Spoleto thrust or Monte Maggio fault, however reaction products of thermally driven decarbonation have been identified along these faults (Collettini et al., 2013, 2014). This may be because decarbonation is occurring at temperatures below what is required for methylphenanthrene reaction in these conditions (~500°C)*

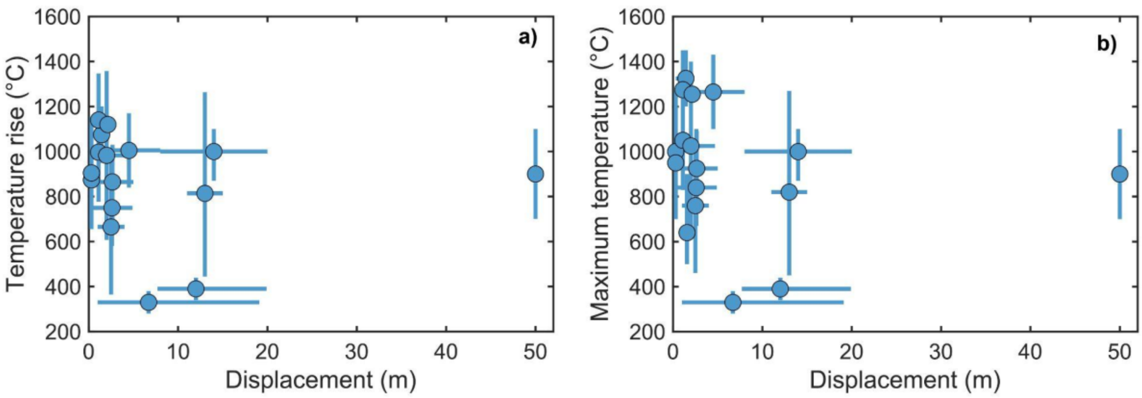

Supplementary Figure 2: Plots of a) temperature rise and b) maximum temperature against earthquake displacement. No clear relationship between coseismic temperature and displacement is apparent.

References

Carpenter, B. M., Scuderi, M. M., Collettini, C., & Marone, C. (2014). Frictional heterogeneities on carbonate-bearing normal faults: Insights from the Monte Maggio Fault, Italy. Journal of Geophysical Research, [Solid Earth], 119(12), 9062–9076.

Collettini, C., Carpenter, B. M., Viti, C., Cruciani, F., Mollo, S., & Tesei, T. (2014). Fault structure and slip localization in carbonate-bearing normal faults: An example from the Northern Apennines of Italy. Journal of Structural Geology, 67, 154–166.

Collettini, C., Viti, C., Tesei, T., & Mollo, S. (2013). Thermal decomposition along natural carbonate faults during earthquakes. Geology, 41, 927–930.

Hecker, S., Abrahamson, N. A., & Wooddell, K. E. (2013). Variability of Displacement at a Point: Implications for Earthquake-Size Distribution and Rupture Hazard on Faults. Bulletin of the Seismological Society of America, 103(2A), 651–674.

Heuze, F. E. (1983, February). High-temperature mechanical, physical and thermal properties of granitic rocks—a review. In International Journal of Rock Mechanics and Mining Sciences & Geomechanics Abstracts (Vol. 20, No. 1, pp. 3-10). Pergamon.

Kirkpatrick, J. D., Dobson, K. J., Mark, D. F., Shipton, Z. K., Brodsky, E. E., & Stuart, F. M. (2012). The depth of pseudotachylyte formation from detailed thermochronology and constraints on coseismic stress drop variability. *Journal of Geophysical Research, [Solid Earth]*, *117*(6), 1–13.

McDermott, R. G., Ault, A. K., Evans, J. P., & Reiners, P. W. (2017). Thermochronometric and textural evidence for seismicity via asperity flash heating on exhumed hematite fault mirrors, Wasatch fault zone, UT, USA. Earth and Planetary Science Letters, 471, 85–93.

Peters, K. E., Walters, C. C., & Moldowan, J. M. (2007). The Biomarker Guide. The Biomarker Guide: Biomarkers and Isotopes in the Environment and Human History, I. https://doi.org/10.1017/CBO9780511524868

Regalla, C. A., Rowe, C. D., Harrichhausen, N., Tarling, M. S., & Singh, J. (2018). Styles of underplating in the Marin Headlands terrane, Franciscan complex, California. Special Paper of the Geological Society of America, 534(10), 155–173.

Sakaguchi, A., Chester, F., Curewitz, D., Fabbri, O., Goldsby, D., Kimura, G., Li, C. F., Masaki, Y., Screaton, E. J., Tsutsumi, A., Ujiie, K., & Yamaguchi, A. (2011). Seismic slip propagation to the updip end of plate boundary subduction interface faults: Vitrinite reflectance geothermometry on integrated ocean drilling program nantro SEIZE cores. *Geology*, *39*(4), 395–398.

Szczerba, M., & Rospondek, M. J. (2010). Controls on distributions of methylphenanthrenes in sedimentary rock extracts: Critical evaluation of existing geochemical data from molecular modelling. Organic Geochemistry, 41(12), 1279–1311.

Ujiie, K., Yamaguchi, H., Sakaguchi, A., & Toh, S. (2007). Pseudotachylytes in an ancient accretionary complex and implications for melt lubrication during subduction zone earthquakes. *Journal of Structural Geology*, *29*(4), 599–613.